Effect of 3d-Metal Doping on Ferromagnetic and Dielectric Properties of Magnetite Thin Films

*Aseya Akbar[1], Saira Riaz[2], Shahid Atiq[3], Zohra N. Kayani[4] and Shahzad Naseem[5]

[1), 2), 3), 5)] *Centre of Excellence in Solid State Physics, University of Punjab, Lahore, Pakistan*
[4)] *Department of Physics, LCWU, Lahore, Pakistan*
[5)] *shahzad.cssp@pu.edu.pk*

ABSTRACT

Among various phases of iron oxide, magnetite (Fe_3O_4) is a promising candidate because of its half metallic nature. Doping of various transition metals in magnetite will alter its electronic and magnetic properties thus extending its field of applications. Sol-gel synthesis of un-doped and chromium doped magnetite thin films are reported in this work. Dopant concentration is varied as 2%, 4%, 6%, 8% and 10%. Presence of diffraction planes (400), (420) and (533) indicates the formation of pure magnetite phase. XRD peak positions shift to higher angles with incorporation of chromium thus leading to contraction of unit cell. Magnetite thin films show ferromagnetic behavior with high saturation magnetization. Chromium substitution results in increase in saturation magnetization up to a dopant concentration of 6%. Variation in magnetization is observed by varying dopant concentration in the range of 2-10%. For low dopant concentration (≤ 6%) Cr^{3+} cations occupy Fe^{3+} cations, while at high dopant concentration >6% decrease in magnetization is associated to arbitrary occupation of chromium on Fe^{3+} and Fe^{2+} sites. Dielectric constant and tangent loss show normal dispersion behavior in accordance with Maxwell Wagner two-layered model. Dielectric constant increases from 216.69 to 529 as dopant concentration is increased to 6%. Further increase in dopant concentration results in decrease in dielectric constant.

1. INTRODUCTION

Magnetite is the material of attention due to its viable magnetic, electronic and structural degrees of freedom along with low temperature transition. Magnetite has found wide technological and industrial applications ranging from spintronic devices to biomedical applications (Hevroni et al. 2016, Akbar et al. 2015, Akbar et al. 2014a, Gracia et al. 2016).

Crystallographic structure of magnetite (Fe_3O_4) is dissimilar from large number of materials due to the existence of two sites: 1) Tetrahedral sites (A-site) and 2) Octahedral sites (B-sites). Magnetite crystallizes in cubic inverse spinel structure. Iron cations are present on both octahedral and tetrahedral sites with general formula $(Fe^{3+})_A[Fe^{3+}Fe^{2+}Fe^{2+}]_BO_4$. Trivalent Fe^{3+} cations ($3d^5$, S=5/2) on A-sites are surrounded by oxygen tetrahedron. On B-sites both Fe^{3+} ($3d^5$, S=5/2) and Fe^{2+} cations ($3d^6$, S=2) are present (Guan et al. 2016, Riaz et al. 2014a). Magnetite possesses Curie

temperature of 855K. Because of the antiparallel alignment of Fe^{3+} cations on octahedral and tetrahedral sites the magnetic moments cancel out and make no contribution to magnetization. The entire contribution to magnetization in magnetite arises from Fe^{2+} cations. The most important advantage that magnetite offers is its half metallic nature. It acts as an insulator for one type of spin, whereas, conductor for other spin orientation (Craik 1975, Garcia et al. 2016).

Because of the presence of both Fe^{2+} and Fe^{3+} cations on octahedral sites magnetite possess relatively high conductivity as compared to other phases of iron oxides (Yazdi et al. 2016, Alraddadi et al. 2016). It undergoes first order transition from poorly conducting to insulating state at low temperature of 119K. This transition, named as Verwey transition, named after scientist E.J.W. Verwey, is accompanied by change in crystallographic structure and latent heat of the material (Varshney and Yogi 2014, Bohra et al. 2016).

Properties of magnetite can be tuned with the help of various dopants that can enable scientists / researchers to extend its range of applications. For this purpose sol-gel along with spin coating method was used to prepare Cr doped magnetite thin films. Dopant concentration was varied as 2%, 4%, 6% and 8%. Variations in structural parameters and their effect on different properties have been explored.

2. EXPERIMENTAL DETAILS

Chromium doped magnetite thin films were prepared using sol-gel method. Iron nitrate was used as precursor and De-ionized (DI) water and ethylene glycol as solvents. Iron nitrate was mixed in DI water and ethylene glycol. The solution was then heat treated on hot plate at 80°C to obtain iron oxide sol. Details of sol-gel synthesis have been reported earlier (Riaz et al. 2014b, Akbar et al. 2014b). For chromium doping, sol of chromium oxide was made separately. This sol was mixed in iron oxide sol to obtain Cr-doped sol with variation in dopant concentration as 2-8%.

Films were deposited on copper substrates. Before coating, substrates were etched in diluted hydrochloric acid. After etching, substrates were ultrasonically agitated in acetone and IPA, separately for 15 minutes (Asghar et al. 2016a,b). Sols were spin coated onto copper substrates at 3000rpm for 30sec. After room temperature aging of films for 24hrs, films were annealed at 300°C.

XRD patterns were determined using Bruker D8 Advance X-ray diffractometer (XRD) with Cuk_{α} radiations (λ = 1.5406Å). For magnetic analysis of iron oxide thin films Lakeshore's 7407 Vibrating Sample Magnetometer (VSM) was used.

3. RESULTS AND DISCUSSION

Fig. 1 shows XRD patterns for Cr doped iron oxide thin films. Peaks are indexed according to JCPDS card no. 72-2303. Occurrence of peaks matched to planes (220), (311), (400), (422) and (533) indicating Fe_3O_4 phase formation. No diffraction peaks associated with Cr_2O_3 were present at 2% and 4% dopant concentration (Fig. 1 (b)). However, at high dopant concentration of 6% peaks associated to Cr_2O_3 were observed. Intensity of Cr_2O_3 peak was enhanced at 8% dopant concentration (Fig. 1 (d)). Displacement of peak positions to high diffraction angles up to a dopant concentration of 4% (Fig. 1 (b)) indicated that Cr^{3+} ions replaced Fe^{3+} cations in the host lattice. However, at high dopant concentration the possibility that Cr^{3+} ions take up

the interstitial sites instead of substitutional sites increases (Biju and Wen 2013, Riaz et al. 2015 Mn doped) thus resulting in inclusion of Cr_2O_3 phase in Fe_3O_4.
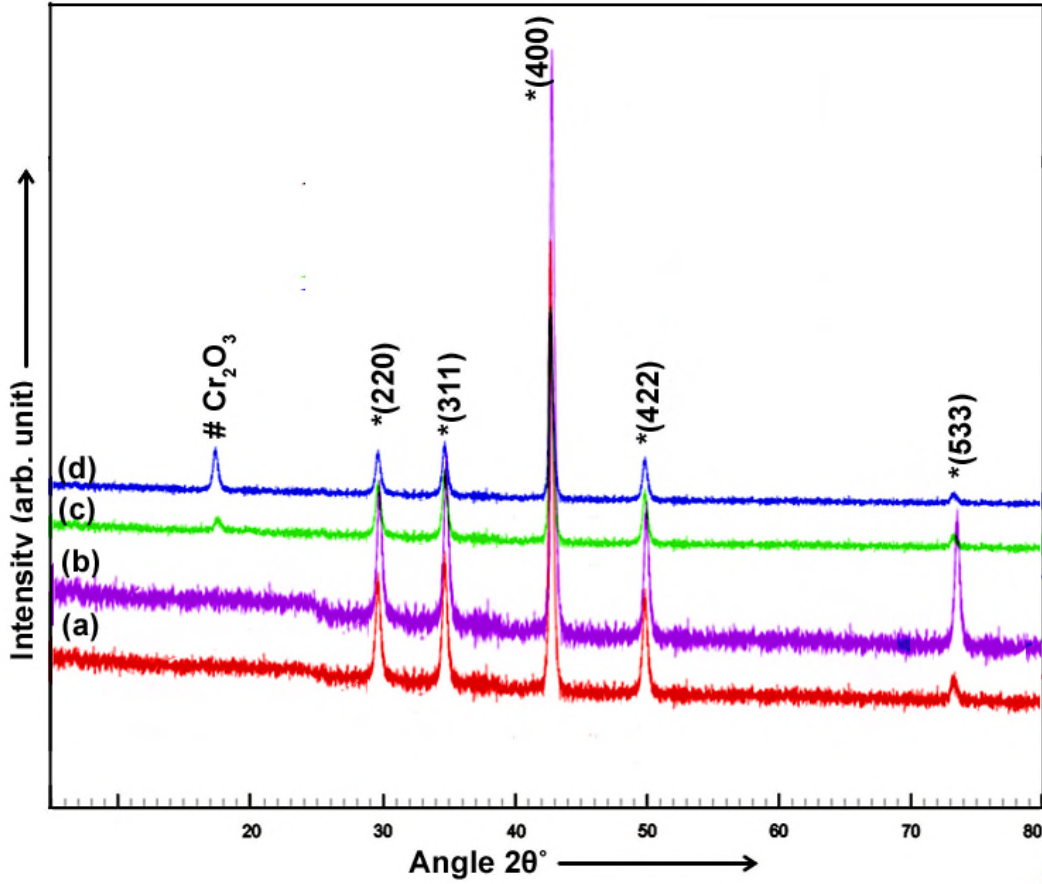

Fig. 1 XRD results for Cr doped Fe_3O_4 thin films with dopant concentration (a) 2% (b) 4% (c) 6% and (d) 8%.

Crystallite size (t), strain (Cullity 1956) and dislocation density (δ) (Kumar et al. 2011) were calculated using Eqs. 1-3.

$$t = \frac{0.9\lambda}{B\cos\theta} \tag{1}$$

$$\delta = \frac{1}{t^2} \tag{2}$$

$$Strain = \frac{\Delta d}{d} = \frac{d_{exp} - d_{hkl}}{d_{hkl}} \tag{3}$$

Where, θ is the diffraction angle, λ represents wavelength (1.5406Å), B is FWHM (Full Width at Half Maximum). d_{exp} is the d-spacing calculated using XRD patterns in Fig. 1 and d_{hkl} is the d-spacing taken from JCPDS card. 72-2303. Crystallite size, strain and dislocation density plots are shown in Fig. 2 (a-b). Crystallite size increased from 27.05nm to 28.53nm as dopant concentration was increased from 2%-

4%. Further increase in dopant concentration to 6% and 8% ended in decrease in crystallite size. Increase in "t" is accredited to development of temperature gradient in the sol owing to replacement of smaller atom (Cr) with atom of larger radius (Fe). This leads to Ostwald Ripening mechanism (Riaz et al. 2015, Azam et al. 2015). Therefore, crystallite size becomes larger as dopant concentration increases to 4%. Further increase in dopant concentration led to a decrease in crystallite size. This decrease might have been observed because of the re-structuring in host lattice because of the appearance of Cr_2O_3 phase. (Riaz and Naseem 2007). It can be seen in Fig. 2 (b) that strain decreased from 2.56×10^{-3} to 2.48×10^{-3} as the dopant concentration was increased from 2% to 4%. This decline in strain energy has also affected the crystallite size (Riaz and Naseem 2007). Enlarged crystallite size is responsible for less number of dislocations in thin films (Fig. 2 (b)). Rise in crystallite size leads to decreased number of grain boundaries (Biju and Wen 2013). For higher dopant concentration i.e. 6% and 8% probability that dopant atoms occupy interstitial sites increases (Biju and Wen 2013) thus resulting in enhanced dislocations and strain in thin films (Fig. 2 (a,b)).
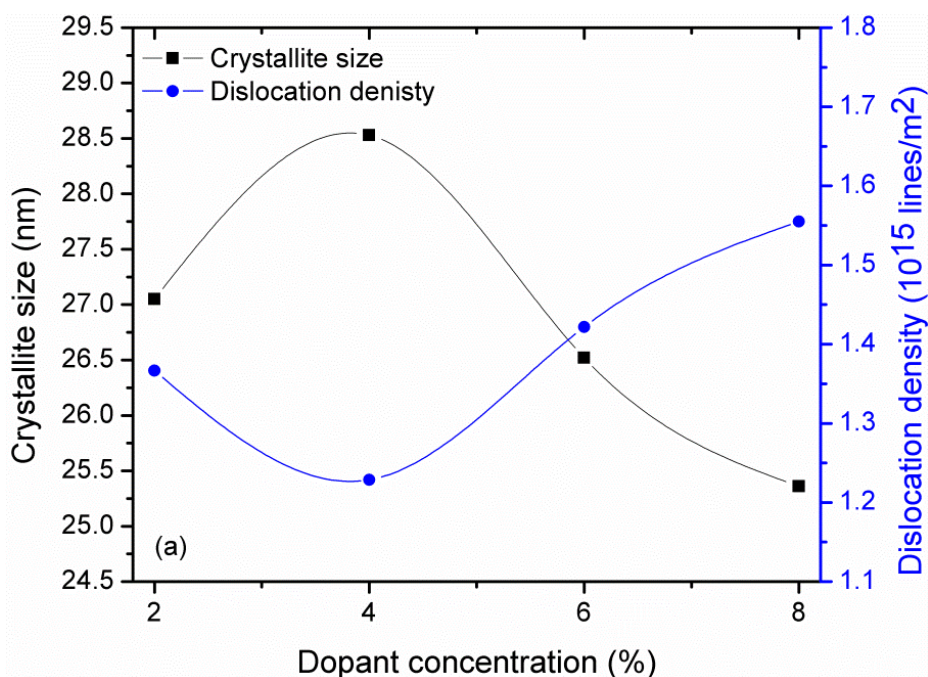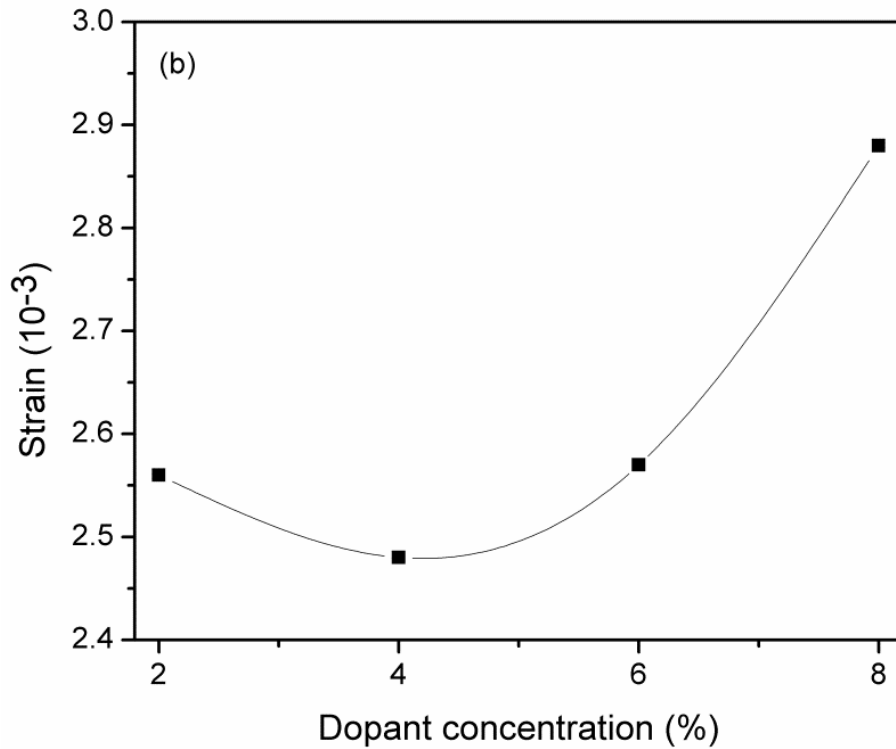
Fig. 2 (a) Crystallite size "t" and dislocation density "δ" (b) strain plotted as a function of dopant concentration

Lattice parameters "a and c ($\AA$)" and x-ray density "ρ (g/cm$^{3)}$" (Cullity 1956) were determined using Eqs. 4-5.

$$\sin^2\theta = \frac{\lambda^2}{4a^2}\left(h^2 + k^2 + l^2\right) \tag{4}$$

$$\rho = \frac{1.66042\,\Sigma A}{V} \tag{5}$$

Lattice parameter and unit cell volume are shown in Fig. 3. It can be seen that "a" and "c" and "V" decreased as dopant concentration was increased to 4%. This decrease in "V" is accredited to dissimilarity in radii of Cr and Fe ions. At high dopant concentration the raise in "V" might have been observed because of the charge repulsion (Riaz et al. 2014c) arising due to Cr_2O_3 phase (Fig. 1 (c,d)).
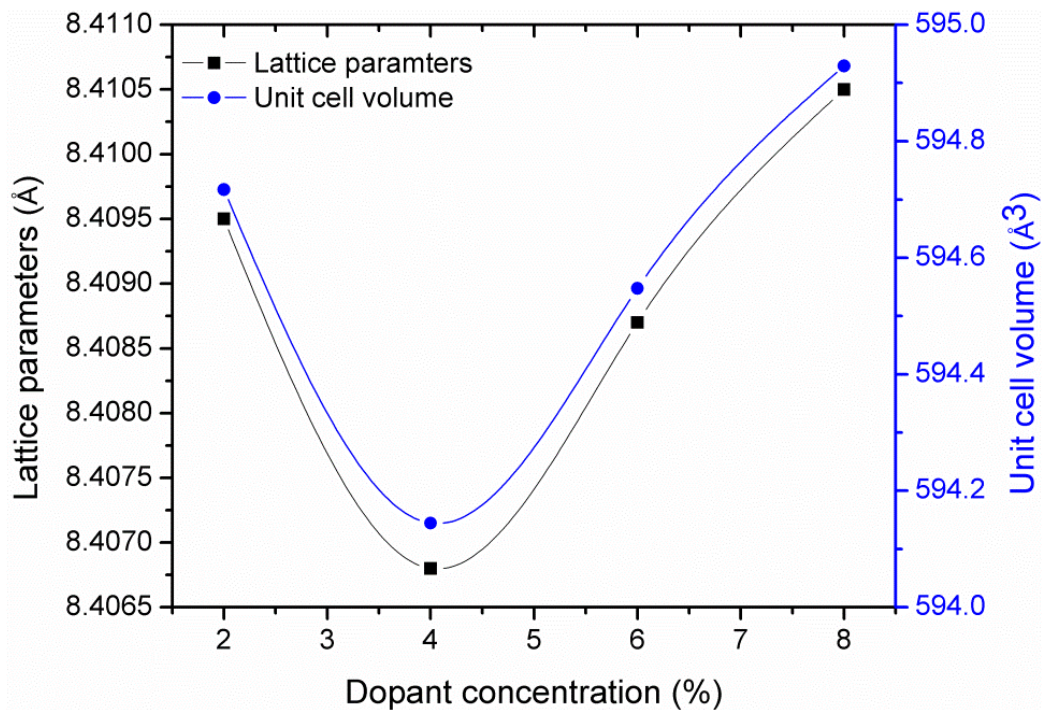
Fig. 3 Lattice parameter "a", "c" and unit cell volume "V" for Cr doped Fe_3O_4 thin films

Fig. 4(a) shows magnetic hysteresis loops for Cr doped Fe_3O_4 thin films. Saturation magnetization "M_s" is shown in Fig. 4(b). "M_s" increased as dopant concentration was raised to 4%. As dopant concentration was further increased to 8% decrease in magnetization arose because of Cr_2O_3 phase (Fig. 1(c,d)). In Fe_3O_4 inverse spinel structure, Fe^{3+} and Fe^{2+} cations practice two different coordination environments: 1) Fe^{2+} and Fe^{3+} with 6-fold coordination (octahedral sites); 2) Fe^{3+} ions with 4-fold coordination (tetrahedral sites). Spins of Fe^{3+} cations are set in antiparallel style on octahedral sites with respect to tetrahedral sites. Thus, Fe^{3+} cations make no contribution to magnetization (Craik 1957). The magnetization in Fe_3O_4 is associated with Fe^{2+} ions. Cr^{3+} ions in Fe_3O_4 can replace both Fe^{2+} and Fe^{3+} cations. So, it is suggested that Cr^{3+} ions should replace Fe^{3+} cations in Fe_3O_4 leading to high Fe^{2+} cations as well as disturbed arrangement of Fe^{3+} and Fe^{2+} ions. As a result of which, improvement in magnetization was observed at low dopant concentration (Fig. 4(b)). This idea is supported by the shift of XRD peak positions to high diffraction angles at low dopant concentration (Fig. 1(c,d)). At high dopant concentration the decrease in saturation magnetization is recognized due to existence of Cr_2O_3 phase (Fig. 1(c,d)) along with arbitrary occupation of chromium on Fe^{3+} and Fe^{2+} sites (Nguyen et al. 2014).
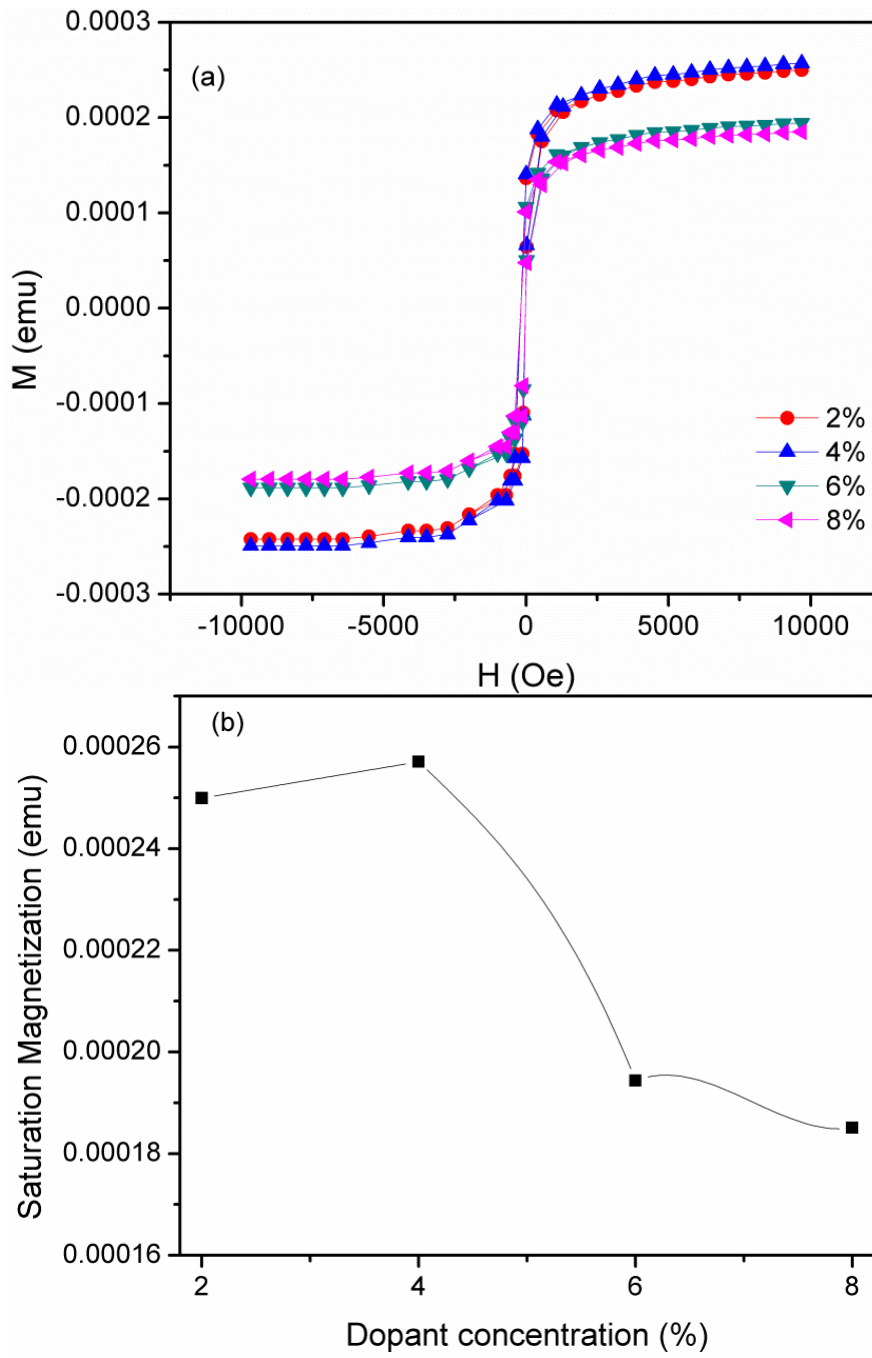
Fig. 4(a) Magnetic curves and (b) "M_s" of Cr doped Fe_3O_4 thin films

Dielectric constant "ε" and tangent loss "$tan\ \delta$)" were determined using Eqs. 6 and 7 (Barsoukov and Macdonald 2005).

$$\varepsilon = \frac{Cd}{\varepsilon_o A} \tag{6}$$

$$\tan\delta = \frac{1}{2\pi f \varepsilon_o \varepsilon \rho} \tag{7}$$

Where, C stands for capacitance of films, d symbolizes film thickness, ε_o indicates permittivity of free space, A represents area, f stands for frequency and ρ indicates resistivity. Variation in dielectric constant and tangent loss is shown in Fig. 5(a,b). This Debye like dispersion is clarified on the basis of Koop's theory. This theory is based on Maxwell-Wagner Model (Riaz et al. 2015, Barsoukov and Macdonald 2005). In addition, an important factor that dictates the dielectric constant and tangent loss in spinel ferrites include electron hopping between Fe^{2+} and Fe^{3+} cations. With changes in frequency the electrons are displaced in the direction of field and hence changes in polarization takes place thus leading to changes in dielectric constant and tangent loss (Barsoukov and Macdonald 2005).
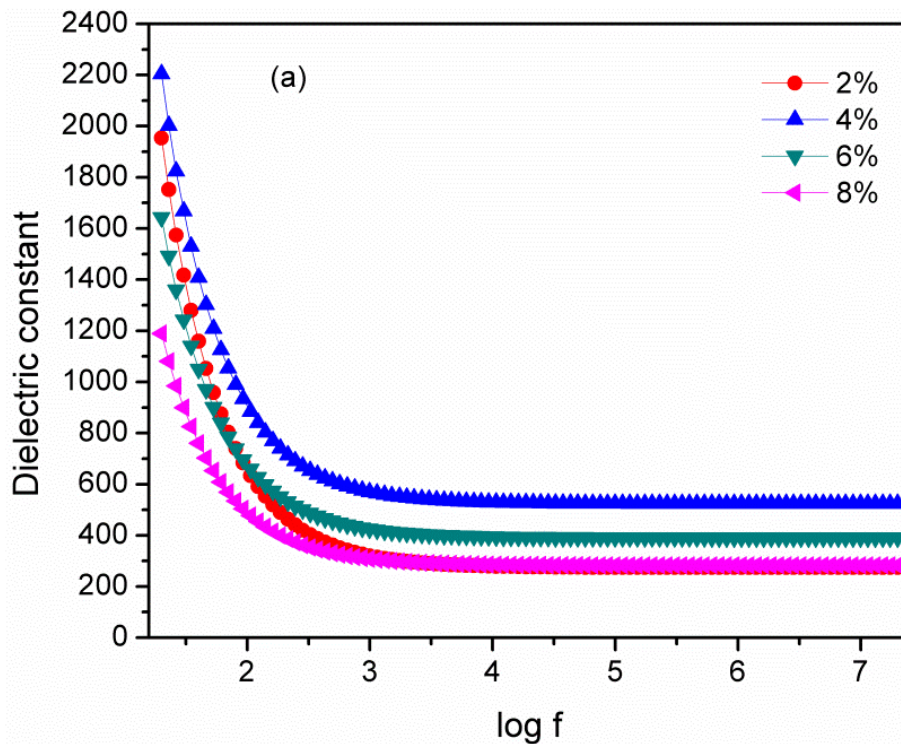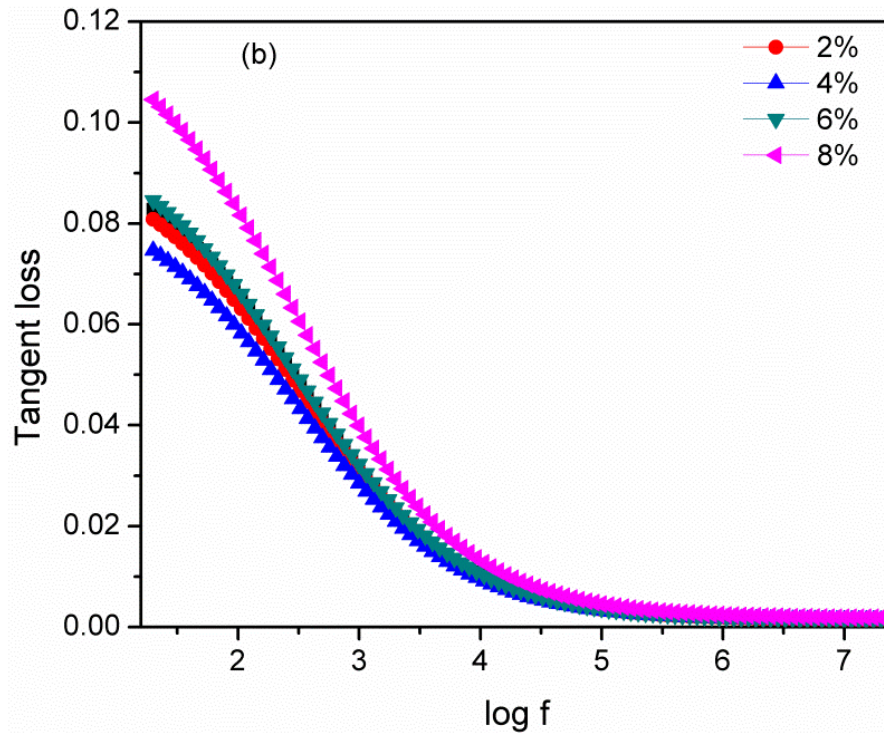
Fig. 5 (a) Dielectric constant "ε" (b) Tangent loss "tanδ" for Cr doped Fe_3O_4 thin films

It can be seen in Fig. 6 that dielectric constant increased from 279.69 to 529 as dopant concentration was increased to 4%. Further increase in dopant level to 8% resulted in decrease in dielectric constant to 285. This decreased value is ascribed to the appearance of Cr_2O_3 phase (Fig. 1). Dielectric constant in thin films is strongly affected by existence of strain. As it was observed in Fig. 2(b) that with incorporation of Cr in the host lattice strain decreased till dopant concentration of 4%. At high dopant concentration arrangement of 180° domains is delayed due to boost in strain (Tang et al. 2013, Riaz et al. 2015) (Fig. 2(b)). In addition, occurrence of secondary phase (Cr_2O_3) at high dopant concentration resulted in decreased $ε$ value and increased $tanδ$.
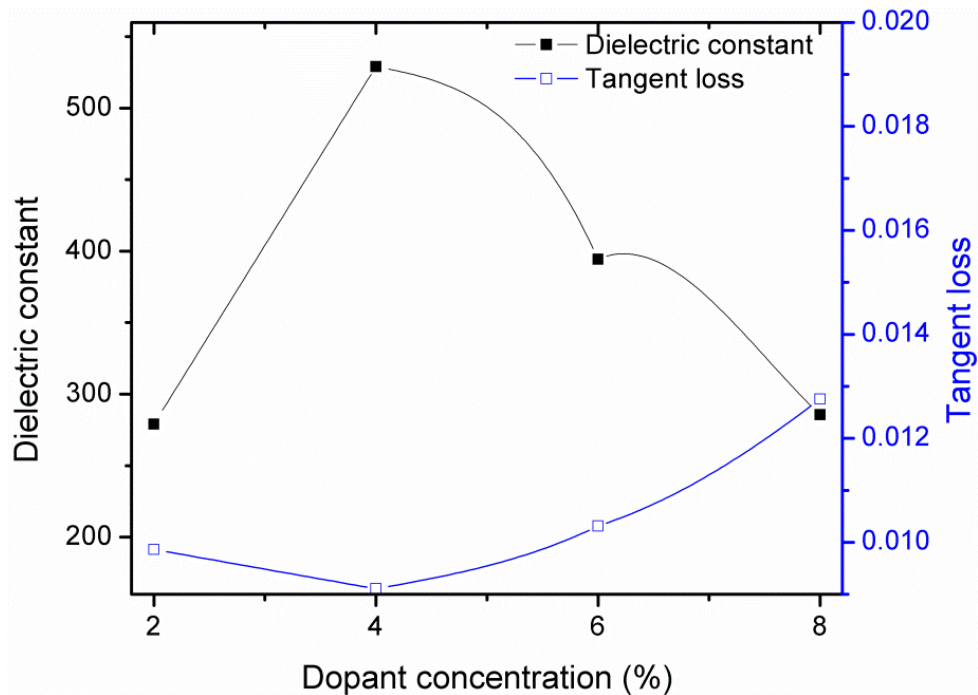
Fig. 6 ε and *tanδ* for Cr doped Fe_3O_4 thin films

4. CONCLUSIONS

Cr doped Fe_3O_4 thin films were deposited via sol-gel spin coating method. Dopant concentration was varied as 2%, 4%, 6% and 8%. XRD results confirmed the formation of Fe_3O_4 phase. With increase in dopant concentration to 4% shifting of peak positions to higher angles indicated successful incorporation of Cr in magnetite lattice. At high dopant concentration (6% and 10%) peaks corresponding to Cr_2O_3 phase were observed. Increase in magnetization at low dopant concentration had been observed because of the replacement of Fe^{3+} cations with Cr^{3+} cations. ε and *tanδ* showed standard dispersion behavior. Increase in dielectric constant was observed from 279.69 to 529 as dopant concentration was increased from 2% to 4%.

REFERENCES

Akbar, A. Riaz, S. Ashraf, R. and Naseem, S. (2014(b)), "Magnetic and magnetization properties of Co-doped Fe_2O_3 thin films", *IEEE Trans. Magn.*, **50**, 2201204.

Akbar, A. Riaz, S. Ashraf, R. and Naseem, S. (2015), "Magnetic and magnetization properties of iron oxide thin films by microwave assisted sol–gel route", *J. Sol-Gel Sci. Technol.*, **74**, 320–328.

Akbar, A. Riaz, S. Bashir, M. and Naseem, S. (2014a), "Effect of Fe^{3+}/Fe^{2+} ratio on superparamagnetic behavior of spin coated iron oxide thin films", *IEEE Trans. Magn.*, **50**, 2200804.

Alraddadi, S. Hines, W. Yilmaz, T. Gu, G.D. and Sinkovic, B. (2016), "Structural phase diagram for ultra-thin epitaxial Fe_3O_4/MgO (0 0 1) films: Thickness and oxygen pressure dependence", *J. Phys.: Condens. Matter*, **28**, 115402.

Asghar, M.H. Placido, F. and Naseem, S. (2006(a)), "Characterization of reactively evaporated TiO_2 thin films as high and medium index layers for optical applications", *Eur. Phys. J. - Appl. Phys.*, **35**, 177-184.

Asghar, M.H. Placido, F. and Naseem, S. (2006(b)), "Characterization of Ta_2O_5 thin films prepared by reactive evaporation", *Eur. Phys. J. - Appl. Phys.*, **36**, 119-124.

Azam. M. Riaz, S. Akbar, A. and Naseem, S. (2015), "Structural, magnetic and dielectric properties of spinel $MgFe_2O_4$ by sol–gel route", *J. Sol-Gel Sci. Technol.*, **74**, 340–351.

Biju, Z. and Wen, H. (2013), "Influence of substrate temperature on the structural and properties of In-doped CdO films prepared by PLD", *J. Semicond.*, **34**, 053003-1-6.

Bohra, M. Prasad, K.E. Bollina, R. Sahoo, S.C. and Kumar, N. (2016), "Characterizing the phase purity of nano crystalline Fe_3O_4 thin films using Verwey transition", *J. Magn. Magn. Mater.*, http://dx.doi.org/10.1016/j.jmmm.2016.02.010.

Craik, D.J. (1975), "Magnetic Oxides", New York: Wiley.

Cullity, B.D. (1956), "Elements of x-ray diffraction," Addison Wesley Publishing Company, USA.

Garcia, L.M. Mascaraque, A. Pabon, B.M. Bliem, R. Parkinson, G.S. Chen, G. Schmid, A.K. and Figuera, J. (2016), "Spin reorientation transition of magnetite (001)," *Phys. Rev. B*, **93**, 134419.

Guan, X. Zhou, G. Xue, W. Quan, Z. and Xu, X. (2016), "The investigation of giant magnetic moment in ultrathin Fe_3O_4 films", *APL Mater.*, **4**, 036104.

Hevroni, A. Bapna, M. Piotrowski, S. Majetich, S.A. and Markovich, G. (2016), "Tracking the Verwey transition in single magnetite nanocrystals by Variable-Temperature Scanning Tunneling Microscopy" *J. Phys. Chem. Lett.*, **7**, 1661−1666.

Kumar, N. Sharma, V. Parihar, U. Sachdeva, R. Padha, N. and Panchal, C.J. (2011), "Structure, optical and electrical characterization of tin selenide thin films deposited at room temperature using thermal evaporation method", *J. Nano- Electron. Phys.*, **3**, 117-126.

Nguyen, H.D. Nguyen, T.D. Nguyen, D.H. and Nguyen, P.T. (2014), "Magnetic properties of Cr doped Fe_3O_4 porous nanoparticles prepared through a coprecipitation method using surfactant", *Adv. Nat. Sci.: Nanosci. Nanotechnol.*, **5,** 035017.

Riaz, S. Akbar, A. and Naseem, S. (2014b), "Ferromagnetic effects in Cr-doped Fe_2O_3 thin films", *IEEE Trans. Magn.*, **50**, 2200704.

Riaz, S. Ashraf, R. Akbar, A. and Naseem, S. (2014a), "Microwave assisted iron oxide nanoparticles—structural and magnetic properties", *IEEE Trans. Magn.*, **50**, 2201504.

Riaz, S. Shah, S.M.H. Akbar, A. Atiq, S. and Naseem, S. (2015), "Effect of Mn doping on structural, dielectric and magnetic properties of $BiFeO_3$ thin films", *J. Sol-Gel Sci. Technol.*, **74**, 329-339.

Riaz, S. Shah, S.M.H. Akbar, A. Kayani, Z.N. and Naseem, S. (2014c), "Effect of Bi/Fe ratio on the structural and magnetic properties of $BiFeO_3$ thin films by Sol-Gel," *IEEE Trans. Magn.*, **50**, 2201304.

Varshney, D. Yogi, A. (2014), "Structural, electrical and magnetoresistance of titanium-doped iron(II,III) oxide (Fe_3O_4) thin films deposited on strontium titanate, alumina, silicon, and float glass", *Mater. Sci. Semicond. Process.*, **26**, 33–40.

Yazdi, M.B. Major, M. Wildes, A. Wilhelm, F. Rogalev, A. Donner, W. Alff, L. (2016), "Possible evidence for a spin-state crossover in the Verwey state in Fe_3O_4 thin films", *Phys. Rev. B*, **93**, 014439.